J. Fluid Mech. (2018), *vol.* 852, *pp.* 37–59. © Cambridge University Press 2018
doi:10.1017/jfm.2018.531

Diffusiophoresis of a charged drop

Fan Yang[1], Sangwoo Shin[2] and Howard A. Stone[1,†]

[1]Department of Mechanical and Aerospace Engineering, Princeton University, Princeton, NJ 08544, USA

[2]Department of Mechanical Engineering, University of Hawaii at Manoa, Honolulu, HI 96822, USA

(Received 10 October 2017; revised 14 February 2018; accepted 27 June 2018;
first published online 2 August 2018)

Diffusiophoresis describes the motion of colloids in an electrolyte or non-electrolyte solution where there is a concentration gradient. While most of the studies of diffusiophoresis focus on the motion of solid particles, soft objects such as drops and bubbles are also known to experience diffusiophoresis. Here, we investigate the diffusiophoresis of charged drops in an electrolyte solution both analytically and experimentally. The drop is assumed to remain spherical. An analytical solution of the diffusiophoretic velocity of drops is obtained by perturbation methods. We find that the flow inside the drop is driven by the tangential electric stress at the interface and it directly influences the diffusiophoretic speed of the drop. Using charged oil droplets, we measure the drop speed under solute concentration gradients and find good agreement with the analytical solution. Our findings have potential applications for oil recovery and drug delivery.

Key words: drops and bubbles, electrohydrodynamic effects

1. Introduction

Colloids immersed in electrolyte solutions usually carry net charges on their surface, which is further surrounded by a cloud of counterions. This cloud, as sketched in figure 1(*a*), is called the 'electric double layer' (EDL) and charged with more counterions than coions. Its typical thickness, also referred as the Debye length, is denoted by κ^{-1}, which is most commonly on the scale of 1–10 nm in water or fluids with high dielectric constants.

If the electrolyte solution has a uniform concentration gradient ∇c_∞, the ion diffusion fluxes $\boldsymbol{j}_{+,D} = -D_+\nabla c_\infty$ and $\boldsymbol{j}_{-,D} = -D_-\nabla c_\infty$ will be different due to differences between the diffusion coefficients of cations (D_+) and anions (D_-). Thus, an electric field $\boldsymbol{E}_\infty$, which accelerates the slowly diffusing ions and decelerates the fast diffusing ions, will build up to maintain the electroneutrality in solution (Prieve *et al.* 1984), as shown in figure 1(*b*). The electric field causes motion of the suspended charged colloids by exerting a force on the fluid inside the EDL, which is the response known as electrophoresis. The solute gradient within the EDL also produces a pressure-driven osmotic flow, which is known as chemiphoresis. The direction of the electro-osmotic flow (EOF) depends on the electric field $\boldsymbol{E}_\infty$ and the charge on the particle/drop surface, while the direction of the chemi-osmotic flow

†Email address for correspondence: hastone@princeton.edu

https://doi.org/10.1017/jfm.2018.531 Published online by Cambridge University Press

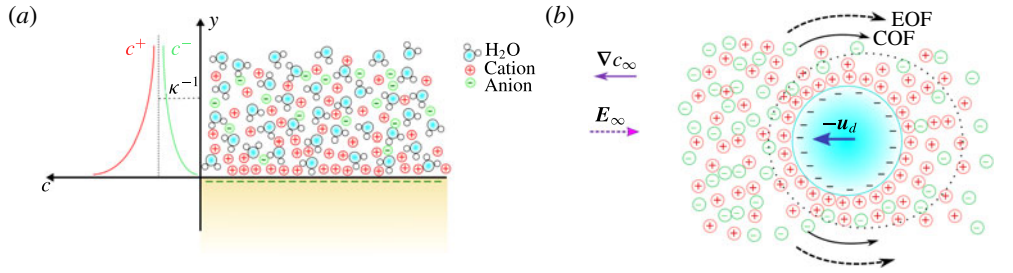

FIGURE 1. (Colour online) (*a*) Electric double layer (EDL): the ratio of the number of water molecules to that of the ions is exaggerated. The former is usually several orders of magnitude higher than the latter in a dilute solution. (*b*) Mechanism of diffusiophoresis when there is an external concentration gradient ∇c_∞. The dotted line indicates the EDL around the colloid. The solid and dotted arrows indicate the directions of the chemi-osmotic flow (COF) and the electro-osmotic flow (EOF), respectively. As a consequence, the velocity of the colloid ($-\boldsymbol{u}_d$) is in the opposite direction in the laboratory frame.

(COF) is always from regions of high-to-low concentration (Prieve *et al.* 1984; Khair & Squires 2009). The interplay of these two forces sets the particle velocity relative to the fluid, i.e. $\boldsymbol{v}_p - \boldsymbol{v}_f = -\boldsymbol{u}_d$, where $\boldsymbol{v}_p$, $\boldsymbol{v}_f$ and $-\boldsymbol{u}_d$ are the particle, local fluid and diffusiophoretic velocity of the particle, respectively.

This mechanism of particle transport, induced by a concentration gradient and consisting of both the electrophoresis and chemiphoresis contributions, is called 'diffusiophoresis', first proposed by Derjaguin *et al.* (1947) and Derjaguin *et al.* (1961). Most of the previous studies of diffusiophoresis are limited to the motion of rigid particles (Prieve *et al.* 1984; Prieve & Roman 1987; Anderson 1989). The viscosity ratio $\overline{\mu}/\mu$ of a drop with viscosity $\overline{\mu}$ and an outer solution with viscosity μ is a key factor in the study of diffusiophoresis of drops; a rigid particle is a special case where $\overline{\mu}/\mu \to \infty$. In the literature, there are only a few papers studying the diffusiophoresis and electrophoresis of drops but they report different results concerning the dependence of the diffusiophoretic speed on $\overline{\mu}/\mu$. For example, Baygents & Saville (1988) calculate the diffusiophoretic speed with different $\overline{\mu}/\mu$, which disagrees the numerical results reported by Lou & Lee (2008). With respect to electrophoresis of droplets of radius a, Booth (1951) and Jordan & Taylor (1952) give different dependence of droplet speed as a function of the imposed uniform electric field on $\overline{\mu}/\mu$ in the limit $\lambda = (\kappa a)^{-1} \to 0$. Additionally, Ohshima & Healy (1984) predict that the electrophoretic speed of a drop does not depend on $\overline{\mu}/\mu$ when the zeta potential on the drop is very large and λ is small, and they refer to this phenomenon as 'solidification' because the drop's diffusiophoretic speed is the same as its equivalent solid particle (same size and zeta potential, but $\overline{\mu}/\mu \to \infty$). However, numerical results reported by Baygents & Saville (1991) show that the 'solidification' effects are more significant when λ increases. For bubbles, Schnitzer, Frankel & Yariv (2014) reports an analysis of electrophoresis of bubbles but the theoretical results are at odds with the experimental observation.

In this paper, we investigate the diffusiophoresis of charged drops both analytically and experimentally. An analytical solution for the diffusiophoretic velocity of non-conductive drops, given in (2.66), is obtained using perturbation methods. In laboratory experiments, we use silicone oil droplets, which are charged by adding ionic surfactants, and measure their speed under a solute concentration gradient. The

https://doi.org/10.1017/jfm.2018.531 Published online by Cambridge University Press

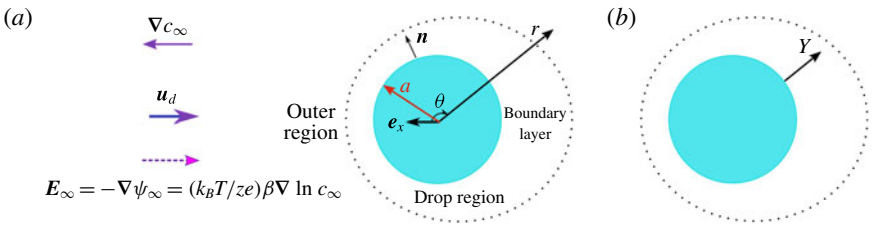

FIGURE 2. (Colour online) (*a*) Model for a spherical drop: the particle surface is charged, either positively or negatively. The dotted line surrounding the particle represents the boundary layer. A spherical coordinate is fixed at the centre of the drop with the direction of $\theta = 0$, namely $\boldsymbol{e}_x$, parallel to ∇c_∞, $\boldsymbol{u}_d$ and $\boldsymbol{E}_\infty$. Also, $\boldsymbol{n}$ is the unit normal vector at the interface. (*b*) The coordinate used in the boundary-layer solutions.

experiments show that the oil droplets move more slowly when $\overline{\mu}/\mu$ decreases. In particular, when the viscosity ratio (drop to continuous phase) $\overline{\mu}/\mu > 10$, the diffusiophoretic speed of oil droplets is almost the same as their equivalent rigid-particle speed. The experimental results are in good agreement with our theory.

The applications of diffusiophoresis have been studied widely (Velegol *et al.* 2016), but often restricted to solid particles, such as transport of colloids to/from a dead-end channel (Kar *et al.* 2015; Shin *et al.* 2016), particle sorting and sample preconcentration (Shin *et al.* 2016), water filtration and purification (Florea *et al.* 2014; Shin *et al.* 2017*b*) and even detecting bone fractures (Yadav *et al.* 2013). Our theory can lay the foundation to extend these applications to droplets, such as is relevant for recovery of oil and drug delivery.

2. Modelling diffusiophoresis of a non-conductive drop

2.1. *Model description*

A spherical coordinate system (r, θ) is fixed to the centre of a sphere of radius a, axisymmetry is assumed and the flow velocity at infinity is denoted by $\boldsymbol{u}_d$. The concentrations of the cations and anions are denoted $c_\pm$, respectively. For simplicity, the valences for both ions are assumed to be the same, denoted by z, such as NaCl (where $z = 1$), KCl, etc. The direction of the concentration gradient is set to be aligned with the axis $\theta = 0$, indicated by a unit vector $\boldsymbol{e}_x$, as shown in figure 2. Therefore, the uniform concentration gradient at $r \to \infty$ is $\nabla c_\infty = G\boldsymbol{e}_x$, where G is the magnitude. Due to symmetry, the direction of $\boldsymbol{u}_d$ should also be along $\boldsymbol{e}_x$.

When the Debye length κ^{-1} is much smaller than the drop radius a, there is a boundary layer (i.e. the EDL) adjacent to the surface of the drop. The whole field is divided into three regions, namely the outer region outside the boundary layer in the bulk solution, the boundary layer adjacent to the drop surface in the continuous phase and the drop region inside the non-conductive drop, as labelled in figure 2(*a*). The corresponding analytical solutions in these regions are called the outer solution, boundary-layer solution and drop-region solution, respectively.

2.2. *Assumptions*

The following assumptions are made in our modelling: (i) there is no solute in the drop; (ii) $\alpha = Ga/c_\infty(0) \ll 1$, where G is the magnitude of the imposed concentration gradient and $c_\infty(0)$ is the solute concentration at $r = 0$ in the absence of the particle,

https://doi.org/10.1017/jfm.2018.531 Published online by Cambridge University Press

which is assumed to be known; (iii) $\lambda = (a\kappa)^{-1} \ll 1$, where κ^{-1} is the Debye length (defined precisely later). The first assumption has a wide application to water–oil systems, because oil is non-polar and most electrolytes dissolve sparingly in it. The second assumption implies that the concentration difference at the scale of the size of drop is much smaller than the background concentration. This limit can be achieved when either the concentration gradient or the size of droplet is sufficiently small. The third assumption requires the electric double layer thickness to be much smaller than the radius of droplet. A typical scale for the Debye length is approximately 1–10 nm in water or fluids with high dielectric constants. A droplet at the scale of 1 μm or larger would typically satisfy $\lambda \ll 1$ very well. In the following analysis, we first use a regular perturbation on α, then for each order of α, a singular perturbation on λ is further applied.

2.3. *Governing equations and boundary conditions*

The ion flux is

$$\boldsymbol{j}_{\pm} = c_{\pm}\boldsymbol{u} - D_{\pm}\left(\nabla c_{\pm} \pm \frac{zec_{\pm}}{k_B T}\nabla\psi\right), \tag{2.1}$$

where $c_+(c_-)$ is the concentration of cations (anions), e is the elementary charge, $\boldsymbol{u}$ is the velocity field, ψ is the electric potential, k_B and T are the Boltzmann constant and the temperature, respectively. Since the flow field $\boldsymbol{u}$ is incompressible, the continuity of ions using (2.1) can be written as

$$D_{\pm}\nabla\cdot\left[\nabla c_{\pm} \pm \frac{ze}{k_B T}c_{\pm}\nabla\psi\right] = \boldsymbol{u}\cdot\nabla c_{\pm} + \frac{\partial c_{\pm}}{\partial t}. \tag{2.2}$$

The governing equation for the electric potential ψ, with electric field $\boldsymbol{E} = -\nabla\psi$, is Gauss's law

$$\nabla^2\psi = -\frac{\rho_e}{\epsilon}, \tag{2.3}$$

where ϵ is the permittivity of the fluid and ρ_e is the local charge density, i.e.

$$\rho_e = ez(c_+ - c_-). \tag{2.4}$$

Finally, because the Reynolds number Re is assumed small, the incompressible flow field is governed by the Stokes equations with an electric body force

$$0 = -\nabla p + \mu\nabla^2\boldsymbol{u} - \rho_e\nabla\psi, \tag{2.5a}$$

$$\nabla\cdot\boldsymbol{u} = 0, \tag{2.5b}$$

where p is the pressure and μ is the viscosity.

The Newtonian stress and Maxwell stress tensors are denoted, respectively, by $\mathcal{S}_N$ and $\mathcal{S}_M$, namely

$$\mathcal{S}_N = -p\boldsymbol{I} + \mu(\nabla\boldsymbol{u} + \nabla\boldsymbol{u}^{\mathrm{T}}), \tag{2.6a}$$

$$\mathcal{S}_M = \epsilon\left[\nabla\psi\nabla\psi - \tfrac{1}{2}(\nabla\psi\cdot\nabla\psi)\boldsymbol{I}\right], \tag{2.6b}$$

where $\boldsymbol{I}$ is the identity tensor. We denote the fields inside the drop with an overbar. At the interface of the drop ($r = a$), we have continuity of velocity and a stress balance (Leal 2007), i.e.

$$\boldsymbol{u} = \overline{\boldsymbol{u}}, \tag{2.7a}$$

$$\boldsymbol{n}\cdot(\mathcal{S}_N + \mathcal{S}_M) - \sigma(\nabla_s\cdot\boldsymbol{n})\boldsymbol{n} + \nabla_s\sigma = \boldsymbol{n}\cdot(\overline{\mathcal{S}}_N + \overline{\mathcal{S}}_M) \tag{2.7b}$$

and for a steady shape,

$$\boldsymbol{n}\cdot\boldsymbol{u} = 0, \tag{2.8}$$

https://doi.org/10.1017/jfm.2018.531 Published online by Cambridge University Press

where $\boldsymbol{n}$ is the unit normal vector at the interface pointing away from the drop into the bulk solution, σ is the surface tension and $\nabla_s = (\boldsymbol{I} - \boldsymbol{nn}) \cdot \nabla$ is the gradient along the surface. We assume there is no surfactant gradient in the solution and thus no surface tension gradient, i.e. $\nabla_s \sigma = \boldsymbol{0}$ in (2.7). Also since there is no solute inside the droplet, the normal ion flux at the interface ($r = a$) should vanish, i.e.

$$\boldsymbol{n} \cdot \boldsymbol{j}_{\pm} = 0. \tag{2.9}$$

The boundary conditions for the electric potential at $r = a$ are

$$\boldsymbol{n} \cdot (\epsilon \nabla \psi - \bar{\epsilon} \nabla \bar{\psi}) = f_e, \tag{2.10a}$$

$$\nabla_s \psi = \nabla_s \bar{\psi} \quad \text{or} \quad \psi = \bar{\psi}, \tag{2.10b}$$

where f_e is the surface charge density and in (2.10*b*) there is no loss of generality setting a constant of integration to be zero.

The boundary condition for the concentration field far from the droplet is

$$\nabla c_+ = \nabla c_- \to \nabla c_\infty = G \boldsymbol{e}_x \quad \text{as } r \to \infty. \tag{2.11}$$

To maintain electroneutrality in the outer region, we should have $\boldsymbol{j}_+ = \boldsymbol{j}_-$, which gives

$$c_+ \boldsymbol{u} - D_+ \left(\nabla c_+ + \frac{z e c_+}{k_B T} \nabla \psi_\infty \right) = c_- \boldsymbol{u} - D_- \left(\nabla c_- - \frac{z e c_-}{k_B T} \nabla \psi_\infty \right). \tag{2.12}$$

Thus, as $r \to \infty$, in accordance with (2.11), equation (2.12) leads to

$$\boldsymbol{E}_\infty = -\nabla \psi_\infty = \frac{k_B T}{z e} \beta \nabla \ln c_\infty, \tag{2.13}$$

where

$$\beta = \frac{D_+ - D_-}{D_+ + D_-}. \tag{2.14}$$

Equation (2.13), together with (2.14), is a classical result derived in Prieve *et al.* (1984). It serves as the boundary condition for the electric field at $r \to \infty$, and explicitly shows how the presence of an ion concentration gradient and a difference of cation and anion diffusivities give rise to a local electric field.

2.4. *Scaling*

The drop radius a is chosen as the typical length scale, so we define $R = r/a$ and the dimensionless gradient operator $\widetilde{\nabla} = a \nabla$. Equation (2.2) gives $\psi = O(k_B T/ze)$. In (2.5*a*), we have $p = O(\epsilon (k_B T/zea)^2)$ using (2.3) to recognize $\rho_e = O(\epsilon k_B T/zea^2)$ and also $u = O(\epsilon (k_B T)^2/\mu a (ze)^2)$. In (2.7), the surface tension is scaled with $\sigma = O(\epsilon/a (k_B T/ze)^2)$ and the dimensionless surface tension is denoted by $\Sigma = \sigma/(\epsilon/a)(k_B T/ze)^2$. In particular, it is useful to note that diffusiophoresis is driven by a concentration gradient, equation (2.11), which in dimensionless terms is $O(\alpha)$. Recalling that $\alpha = Ga/c_\infty \ll 1$, we now assume a regular perturbation series in α, i.e.

$$c_\pm = c_\infty(0)(C_{0\pm} + \alpha C_{1\pm} + O(\alpha^2)), \tag{2.15a}$$

$$\psi = \frac{k_B T}{ze}(\Psi_0 + \alpha \Psi_1 + O(\alpha^2)), \tag{2.15b}$$

https://doi.org/10.1017/jfm.2018.531 Published online by Cambridge University Press

$$\boldsymbol{u} = \frac{\epsilon (k_B T)^2}{\mu a (ze)^2}(0 + \alpha \boldsymbol{U}_1 + O(\alpha^2)) = \frac{\alpha \epsilon (k_B T)^2}{\mu a (ze)^2}\boldsymbol{U}_1 + O(\alpha^2), \tag{2.15c}$$

$$p = \epsilon \left(\frac{k_B T}{zea}\right)^2 (P_0 + \alpha P_1 + O(\alpha^2)). \tag{2.15d}$$

The surface charge density f_e can be non-dimensionalized by $zec_\infty(0)a$, and expanded as

$$f_e = zec_\infty(0)a(F_0 + \alpha F_1 + O(\alpha^2)). \tag{2.16}$$

With this notation, the capital letters are non-dimensionalized with the subscript indicating the order of α. Note that $\boldsymbol{U}_0 = \boldsymbol{0}$ in (2.15*c*) because the flow field is induced by the concentration gradient. Also, the contribution of the deformation of a spherical drop to its velocity is $O(\epsilon E^2 a/\sigma)$ (Mandal, Bandopadhyay & Chakraborty 2016), which is the electric capillary number. With the orders of magnitude indicated in (2.15), the electric capillary number is $\alpha\epsilon/a\sigma(k_B T/ze)^2 \ll 1$ (for silicone oil droplets with radius 1 μm in water at room temperature, $\epsilon/a\sigma(k_B T/ze)^2 = O(10^{-5})$). Thus, the deformation of the drop can be neglected.

In the following analysis, we use both a regular perturbation on α, as above, and a singular perturbation on $\lambda = (a\kappa)^{-1} \ll 1$ to solve the governing equations. For example, as shown in (2.33) below, the $O(\alpha^0)$ for the electric potential Ψ can be further expanded as a series of λ, i.e.

$$\Psi_0 = \Psi_0^{(0)} + \lambda \Psi_0^{(1)} + O(\lambda^2), \tag{2.17}$$

where the superscript 'n' indicates the order of expansion in λ (and the subscript is the order of expansion in α). This expansion in λ can be similarly applied to any field variable at any order of α. We next construct solutions to the governing equations.

2.5. $O(\alpha^0)$ and $O(\alpha, \lambda^0)$ outer solutions of the concentration and electric fields

The $O(\alpha^0)$ of both the concentration field and electric potential are constant in the absence of the particle and the concentration gradient. The constant concentration field is $c_\infty(0)$ in dimensional form or 1 in dimensionless form, as shown in (2.15*a*); the constant undisturbed electric potential is defined by $\Psi_\infty(0)$, i.e.

$$C_{o,0+} = C_{o,0-} = C_{o,0} = 1, \tag{2.18a}$$

$$\Psi_{o,0} = \Psi_\infty(0), \tag{2.18b}$$

where the subscript 'o' represents the outer solution and $C_{o,0}$ is the concentration field for both cations and anions in the outer region at $O(\alpha^0)$.

At $O(\alpha)$, there is no net charge in the outer region, therefore, the Poisson equation (2.3) becomes

$$\widetilde{\nabla}^2 \Psi_{o,1} = 0. \tag{2.19}$$

The concentration field in the outer region should satisfy

$$C_{o,1+} = C_{o,1-} = C_{o,1}, \tag{2.20}$$

where $C_{o,1}$ is the concentration field for both cations and anions in the outer region at $O(\alpha)$. If we neglect the convective term in (2.2), the continuity of ions leads to

$$\widetilde{\nabla}^2 C_{o,1} = 0. \tag{2.21}$$

https://doi.org/10.1017/jfm.2018.531 Published online by Cambridge University Press

Neglecting the convection can be justified by assuming the Péclet number $Pe = ua/D \ll 1$. Based on the scaling identified in § 2.4, the Péclet number is given by

$$Pe = \alpha \frac{\epsilon (k_B T)^2}{\mu D^* (ze)^2}, \tag{2.22}$$

where we assume D_+ and D_- are of the same order of magnitude, indicated by D^*. An estimate for Pe/α using $D^* = 10^{-9}$ m^2 s^{-1}, $T = 300$ K and $z = 1$ shows that $Pe/\alpha \simeq 0.5$ for water. Thus, the convective term, as characterized by Pe, for ion transport can be neglected when $\alpha \ll 1$.

By matching with (2.11), the boundary conditions for the concentration field in the outer region at $O(\alpha, \lambda^0)$ are

$$\widetilde{\nabla} C_{o,1}^{(0)} \to \boldsymbol{e}_x \quad \text{as } R \to \infty, \tag{2.23a}$$

$$\boldsymbol{n} \cdot \widetilde{\nabla} C_{o,1}^{(0)} = 0 \quad \text{at } R = 1^+, \tag{2.23b}$$

where $R = 1^+$ indicates the outer boundary of the EDL at the drop surface. We note that (2.23*b*) is based on the assumption that there are no solutes inside the droplet and consequently the normal ion flux at the interface is $O(\lambda)$ (Anderson & Prieve 1991; Pawar, Solomentsev & Anderson 1993). Therefore, in the limit $\lambda \to 0$, the normal flux at the outer boundary of the EDL can be neglected. Also, up to $O(\lambda^0)$, $R = 1^+$ can be replaced by $R = 1$ in (2.23*b*). With these assumptions, the solution of (2.21) with (2.23) is

$$C_{o,1}^{(0)}(R, \theta) = \left(1 + \frac{1}{2R^3}\right) \boldsymbol{R} \cdot \boldsymbol{e}_x. \tag{2.24}$$

This solution is the outer concentration field at $O(\alpha, \lambda^0)$. Similarly the boundary conditions for the electric field in the outer region at $O(\alpha, \lambda^0)$ are

$$\widetilde{\nabla} \Psi_o^{(0)} \to \widetilde{\nabla} \Psi_\infty \quad \text{as } R \to \infty, \tag{2.25a}$$

$$\boldsymbol{n} \cdot \widetilde{\nabla} \Psi_o^{(0)} = 0 \quad \text{at } R = 1^+, \tag{2.25b}$$

where $\Psi_\infty = ze\psi_\infty / k_B T$ is the dimensionless electric potential in the far field. The outer solution of (2.19) with (2.13) and (2.25) for the electric potential at $O(\alpha, \lambda^0)$ is

$$\Psi_{o,1}^{(0)}(r, \theta) = -\beta \left(1 + \frac{1}{2R^3}\right) \boldsymbol{R} \cdot \boldsymbol{e}_x. \tag{2.26}$$

In the following sections, we proceed to calculate the flow field and the boundary-layer and drop-region solutions for the concentration field and electric potential using perturbation expansions. Our calculation follows Prieve *et al.* (1984) to solve for the flow field outside the droplet. By applying the boundary conditions at the interface (2.7), we can calculate the induced flow field inside the drop and so analyse its effect on the diffusiophoretic speed of a drop. The theory is then compared with experimental measurements in § 3.

2.6. $O(\alpha^0)$ *solutions of the concentration and electric fields in the boundary layer and drop region*

At $O(\alpha^0)$, there is no ion flux in a steady state inside the boundary layer in the absence of an imposed concentration gradient in the outer region, and the ion flux also

https://doi.org/10.1017/jfm.2018.531 Published online by Cambridge University Press

vanishes inside the drop because there is no solute. Therefore, in both the boundary layer and drop region, we have

$$\boldsymbol{j}_{0\pm} = \boldsymbol{0}. \tag{2.27}$$

The zeroth-order approximations in an expansion in α for (2.1), (2.3), (2.4) and (2.27) are

$$\widetilde{\nabla} C_{0\pm} \pm C_{0\pm} \widetilde{\nabla} \Psi_0 = \boldsymbol{0}, \tag{2.28a}$$

$$\widetilde{\nabla}^2 \Psi_0 = \frac{a^2 z^2 e^2 c_0}{\epsilon k_B T}(C_{0-} - C_{0+}) = \frac{1}{2\lambda^2}(C_{0-} - C_{0+}). \tag{2.28b}$$

We note that at this level of approximation there are no flow effects. The expression for the Debye length can be determined from (2.28*b*) with $\lambda = (a\kappa)^{-1}$, i.e.

$$\kappa^{-1} = \sqrt{\frac{\epsilon k_B T}{2z^2 e^2 c_0}}. \tag{2.29}$$

Now we determine the boundary-layer solutions using a perturbation approach based on $\lambda \ll 1$. By rescaling the radial coordinate by $Y = \lambda^{-1}(R - 1)$, as shown in figure 2(*b*), a boundary layer is introduced on the drop surface, which is the EDL. We denote the boundary-layer solutions with an additional subscript '*b*', i.e.

$$C_{0\pm}(R) = C_{0\pm}(\lambda Y + 1) = C_{b,0\pm}(Y), \tag{2.30a}$$

$$\Psi_0(R) = \Psi_0(\lambda Y + 1) = \Psi_{b,0}(Y). \tag{2.30b}$$

Equations (2.30) define the function $C_{b,0\pm}$ and $\Psi_{b,0}$. By asymptotically matching with the outer solutions at $O(\alpha^0)$ (2.18), the boundary conditions are

$$C_{b,0\pm} \to 1 \quad \text{as } Y \to \infty, \tag{2.31a}$$

$$\Psi_{b,0} \to \Psi_\infty(0) \quad \text{as } Y \to \infty, \tag{2.31b}$$

$$\Psi_{b,0} = \frac{ze\zeta}{k_B T} + \Psi_\infty(0) \quad \text{at } Y = 0, \tag{2.31c}$$

where ζ is the zeta potential of the drop.

The solution of (2.28*a*) is familiar,

$$C_{b,0\pm} = \mathrm{e}^{\mp(\Psi_{b,0} - \Psi_\infty(0))}. \tag{2.32}$$

The boundary-layer solutions for the electric potential based on solving (2.28*b*) with (2.31*b*) and (2.31*c*) are given in Chew & Sen (1982) as a singular perturbation expansion in $\lambda \ll 1$. The results are

$$\Psi_{b,0} = \Psi_{b,0}^{(0)} + \lambda \Psi_{b,0}^{(1)} + O(\lambda^2), \tag{2.33a}$$

$$\text{where} \quad \Psi_{b,0}^{(0)} = \Psi_\infty(0) + 4\ \operatorname{arctanh}(\gamma \mathrm{e}^{-Y}), \tag{2.33b}$$

$$\text{and} \quad \Psi_{b,0}^{(1)} = \frac{2\gamma \mathrm{e}^{-Y}}{1 - \gamma^2 \mathrm{e}^{-2Y}}[\gamma^2(1 - \mathrm{e}^{-2Y}) - 2Y], \tag{2.33c}$$

with the constant

$$\gamma = \tanh\frac{ze\zeta}{4k_B T}. \tag{2.34}$$

Recall that the superscript '*n*' indicates a term $O(\lambda^n)$.

https://doi.org/10.1017/jfm.2018.531 Published online by Cambridge University Press

In the drop region, i.e. the domain inside the drop, since there is no solute, the electric potential $\overline{\Psi}_0$ is governed by

$$\widetilde{\nabla}^2\overline{\Psi}_0 = 0 \tag{2.35}$$

and the boundary conditions are

$$\overline{\Psi}_0 = \frac{ze\zeta}{k_BT} + \Psi_\infty(0) \quad \text{at } R = 1, \tag{2.36a}$$

$$\frac{\mathrm{d}\overline{\Psi}_0}{\mathrm{d}R} \text{ bounded at } R = 0. \tag{2.36b}$$

The solution for $\overline{\Psi}_0(R)$ is a constant, i.e.

$$\overline{\Psi}_0(R) = \frac{ze\zeta}{k_BT} + \Psi_\infty(0), \quad \text{at } 0 \leqslant R \leqslant 1. \tag{2.37}$$

2.7. $O(\alpha, \lambda^0)$ *solutions of the velocity field in all regions and the concentration and electric fields in the boundary layer and drop region*

We now proceed to the next order to calculate the velocity field from which the translation speed of the drop is determined. The $O(\alpha)$ term of the ion transport equation (2.2) is

$$\omega_\pm\widetilde{\nabla}\cdot[\widetilde{\nabla}C_{1\pm} \pm C_{0\pm}\widetilde{\nabla}\Psi_1 \pm C_{1\pm}\widetilde{\nabla}\Psi_0] = Pe_b\boldsymbol{U}_1\cdot\widetilde{\nabla}C_{0\pm}, \tag{2.38}$$

where $\omega_\pm = D_\pm/D = 1/1 \mp \beta$ is the dimensionless diffusion coefficient with $D = 2D_+D_-/D_+ + D_-$. The constant Pe_b, which plays the role of a Péclet number, is

$$Pe_b = \frac{\epsilon(k_BT)^2}{\mu D(ze)^2}. \tag{2.39}$$

Also notice that the transient term in (2.2) is neglected since $\partial c/\partial t \approx (\partial c/\partial x)(\partial x/\partial t) = O(\alpha^2)$. The $O(\alpha)$ term of Gauss's law (2.3) is

$$\widetilde{\nabla}^2\Psi_1 = \frac{a^2z^2e^2c_\infty}{\epsilon k_BT}(C_{1-} - C_{1+}) = \frac{1}{2\lambda^2}(C_{1-} - C_{1+}). \tag{2.40}$$

Taking the curl of (2.5*a*), the $O(\alpha)$ equation is

$$0 = \widetilde{\nabla}\wedge\widetilde{\nabla}^2\boldsymbol{U}_1 + \widetilde{\nabla}\wedge(\widetilde{\nabla}^2\Psi_0\widetilde{\nabla}\Psi_1 + \widetilde{\nabla}^2\Psi_1\widetilde{\nabla}\Psi_0). \tag{2.41}$$

By defining $\boldsymbol{U}_1 = U_r\boldsymbol{e}_r + U_\theta\boldsymbol{e}_\theta$, where U_r and U_θ are the radial and angular velocity, respectively, the continuity equation can be written as

$$\frac{1}{R^2}\frac{\partial}{\partial R}(R^2U_r) + \frac{1}{R\sin\theta}\frac{\partial}{\partial\theta}(U_\theta\sin\theta) = 0. \tag{2.42}$$

The far-field boundary conditions for the concentration and electric fields in the outer region are found by matching with (2.24) and (2.26) at $R\to\infty$, i.e.

$$C_{1\pm} \to R\cos\theta, \tag{2.43a}$$

$$\Psi_1 \to -\beta R\cos\theta, \tag{2.43b}$$

$$U_r \to -U_d\cos\theta, \tag{2.43c}$$

$$U_\theta \to U_d\sin\theta \tag{2.43d}$$

https://doi.org/10.1017/jfm.2018.531 Published online by Cambridge University Press

and $U_d = \epsilon(k_B T)^2/\mu a(ze)^2 \boldsymbol{u}_d \cdot \boldsymbol{e}_x$ is the dimensionless speed in the far field for which we want to solve. The concentration and electric potential fields vary linearly with position while the far-field velocity is uniform.

It is easy to check (Baygents & Saville 1988) that the radial and angular velocities can be decomposed into

$$U_r(R, \theta) = \mathcal{U}(R)\cos\theta, \tag{2.44a}$$
$$U_\theta(R, \theta) = \mathcal{V}(R)\sin\theta \tag{2.44b}$$

and they will satisfy the continuity equation and boundary conditions. Similarly, we can also assume

$$C_{1\pm}(R, \theta) = \mathcal{C}_\pm(R)\cos\theta, \tag{2.45a}$$
$$\Psi_1(R, \theta) = \Phi(R)\cos\theta. \tag{2.45b}$$

Inside the boundary layer, we use a singular perturbation on λ and let $Y = \lambda^{-1}(R-1)$. The field variables in the boundary layer are defined by changing variable from R to Y, i.e.

$$U_r = \mathcal{U}(\lambda Y + 1)\cos\theta = \mathcal{U}_b(Y)\cos\theta, \tag{2.46a}$$
$$U_\theta = \mathcal{V}(\lambda Y + 1)\sin\theta = \mathcal{V}_b(Y)\sin\theta, \tag{2.46b}$$
$$C_{1\pm} = \mathcal{C}_\pm(\lambda Y + 1)\cos\theta = \mathcal{C}_{b,\pm}(Y)\cos\theta, \tag{2.46c}$$
$$\Psi_1 = \Phi(\lambda Y + 1)\cos\theta = \Phi_b(Y)\cos\theta. \tag{2.46d}$$

Next we expand all the functions in terms of λ, i.e.

$$\mathcal{U}_b = \mathcal{U}_b^{(0)} + \lambda\mathcal{U}_b^{(1)} + O(\lambda^2), \tag{2.47a}$$
$$\mathcal{V}_b = \mathcal{V}_b^{(0)} + \lambda\mathcal{V}_b^{(1)} + O(\lambda^2). \tag{2.47b}$$

Similar methods in Prieve *et al.* (1984) are employed to solve the velocity field inside the boundary layer. The details are provided in appendix A. The results are

$$\mathcal{U}_b^{(0)}(Y) = 0, \tag{2.48a}$$
$$\mathcal{V}_b^{(0)}(Y) = 3(1-\beta)[\ln(\mathrm{e}^Y + \gamma) - Y] + 3(1+\beta)[\ln(\mathrm{e}^Y - \gamma) - Y] + C_V, \tag{2.48b}$$

where C_V is a constant to be determined.

When solving for the outer solution of the momentum equation, due to electroneutrality, we only need to solve the homogeneous Stokes' equations. Thus, the outer solution has the form

$$\mathcal{U}_o(R) = \frac{a_1}{R^3} + \frac{a_2}{R} + a_3 + a_4 R^2, \tag{2.49a}$$
$$\mathcal{V}_o(R) = \frac{a_1}{2R^3} - \frac{a_2}{2R} - a_3 - 2a_4 R^2, \tag{2.49b}$$

where a_1, a_2, a_3 and a_4 are constants, and $\mathcal{U}_o(R)$ and $\mathcal{V}_o(R)$ are the outer solutions for $\mathcal{U}(R)$ and $\mathcal{V}(R)$ in (2.44), respectively. To satisfy boundary conditions (2.43*c*) and (2.43*d*), we have

$$a_3 = -U_d, \tag{2.50a}$$
$$a_4 = 0. \tag{2.50b}$$

https://doi.org/10.1017/jfm.2018.531 Published online by Cambridge University Press

It can be shown that the electric force on any closed surface around a sphere in the outer region is zero up to $O(\alpha)$ (Prieve *et al.* 1984), and the hydrodynamic force on the drop (together with the EDL) is proportional to a_2 (Happel & Brenner 1973). Therefore, the force balance gives that $a_2 = 0$ at $O(\alpha)$ and (2.49) becomes

$$\mathcal{U}_o(R) = \frac{a_1}{R^3} - U_d, \tag{2.51a}$$

$$\mathcal{V}_o(R) = \frac{a_1}{2R^3} + U_d. \tag{2.51b}$$

By matching with the boundary-layer solutions (2.48) at the interface, we have

$$a_1^{(0)} - U_d^{(0)} = 0, \tag{2.52a}$$

$$\frac{a_1^{(0)}}{2} + U_d^{(0)} = C_V. \tag{2.52b}$$

Thus,

$$U_d^{(0)} = \frac{2C_V}{3}. \tag{2.53}$$

Similarly, the drop-region solutions for the velocity field have the form

$$\overline{\mathcal{U}}(R) = \frac{\overline{a}_1}{R^3} + \frac{\overline{a}_2}{R} + \overline{a}_3 + \overline{a}_4 R^2, \tag{2.54a}$$

$$\overline{\mathcal{V}}(R) = \frac{\overline{a}_1}{2R^3} - \frac{\overline{a}_2}{2R} - \overline{a}_3 - 2\overline{a}_4 R^2, \tag{2.54b}$$

where $\overline{a}_1$, $\overline{a}_2$, $\overline{a}_3$ and $\overline{a}_4$ are constants. The boundedness at $R = 0$ requires that $\overline{a}_1 = \overline{a}_2 = 0$. By matching with boundary-layer solutions (2.48), we have

$$\overline{a}_4^{(0)} = -\overline{a}_3^{(0)} = -3(1-\beta)\ln(1+\gamma) - 3(1+\beta)\ln(1-\gamma) - C_V. \tag{2.55}$$

Therefore,

$$\overline{\mathcal{U}}^{(0)}(R) = \overline{a}_4^{(0)}(R^2 - 1), \tag{2.56a}$$

$$\overline{\mathcal{V}}^{(0)}(R) = -\overline{a}_4^{(0)}(2R^2 - 1). \tag{2.56b}$$

The $O(\alpha)$ contribution to the tangential component of the stress-balance boundary condition (2.7) including electrical effects is

$$\frac{1}{R}\frac{\partial U_r}{\partial \theta} - \frac{U_\theta}{R} + \frac{\partial U_\theta}{\partial R} + \frac{1}{R}\frac{\mathrm{d}\Psi_0}{\mathrm{d}R}\frac{\partial \Psi_1}{\partial \theta} = \frac{\overline{\mu}}{\mu}\left(\frac{1}{R}\frac{\partial \overline{U}_r}{\partial \theta} - \frac{\overline{U}_\theta}{R} + \frac{\partial \overline{U}_\theta}{\partial R}\right) + \frac{\overline{\epsilon}}{\epsilon R}\frac{\mathrm{d}\overline{\Psi}_0}{\mathrm{d}R}\frac{\partial \overline{\Psi}_1}{\partial \theta}. \tag{2.57}$$

Applying the boundary conditions for the electric potential (2.10*a*) at the interface

$$\frac{\mathrm{d}\Psi_0}{\mathrm{d}R} - \frac{\overline{\epsilon}}{\epsilon}\frac{\mathrm{d}\overline{\Psi}_0}{\mathrm{d}R} = \frac{1}{2\lambda^2}F_0, \tag{2.58a}$$

$$\Psi_1 = \overline{\Psi}_1, \tag{2.58b}$$

as well as

$$U_r = \overline{U}_r = 0, \tag{2.59}$$

https://doi.org/10.1017/jfm.2018.531 Published online by Cambridge University Press

then substituting into (2.57), we have

$$-U_\theta + \frac{\partial U_\theta}{\partial R} + \lambda^{-1} F_0 \frac{\partial \Psi_1}{\partial \theta} = \frac{\overline{\mu}}{\mu}\left(-\overline{U}_\theta + \frac{\partial \overline{U}_\theta}{\partial R}\right), \tag{2.60}$$

where F_0 is the dimensionless surface charge density at $O(\alpha^0)$. Together with (2.33) and (2.37), F_0 can be calculated through (2.58*a*), which is

$$F_0 = F_0^{(0)} + \lambda F_0^{(1)} + \lambda^2 F_0^{(2)} + O(\lambda^3) \tag{2.61}$$

with

$$F_0^{(0)} = 0, \tag{2.62a}$$

$$F_0^{(1)} = -\frac{8\gamma}{1-\gamma^2}, \tag{2.62b}$$

$$F_0^{(2)} = -8\gamma. \tag{2.62c}$$

Substituting (2.46*b*), (A 19), (2.48*b*) and (2.56*b*) into (2.57), we have

$$\begin{aligned} &3\lambda^{-1}\left(-\frac{(1-\beta)\gamma}{1+\gamma} + \frac{(1+\beta)\gamma}{1-\gamma}\right) - 3(1-\beta)\ln(1+\gamma) - 3(1+\beta)\ln(1-\gamma) \\ &- C_V - \left[\lambda^{-1}\frac{4\gamma}{1-\gamma^2} + 4\gamma\right]\left[\Phi^{(0)}(0) + \lambda\Phi^{(1)}(0)\right] = -3\frac{\overline{\mu}}{\mu}\overline{a}_{4,0}. \end{aligned} \tag{2.63}$$

Thus by asymptotically matching orders of λ, we find

$$\Phi^{(0)}(0) = \frac{3(\gamma+\beta)}{2}, \tag{2.64a}$$

$$-3(1-\beta)\ln(1+\gamma) - 3(1+\beta)\ln(1-\gamma) - C_V - 4\gamma\Phi^{(0)}(0) - \frac{4\gamma\Phi^{(1)}(0)}{1-\gamma^2} = -3\frac{\overline{\mu}}{\mu}\overline{a}_{4,0}. \tag{2.64b}$$

Then, using (2.53) and (2.55), we obtain

$$\overline{a}_4^{(0)} = -\frac{1}{1+3\overline{\mu}/\mu}\left[6\gamma(\gamma+\beta) + \frac{4\gamma\Phi^{(1)}(0)}{1-\gamma^2}\right] \tag{2.65}$$

and

$$U_d^{(0)} = \frac{2}{3}C_V = -2\ln(1-\gamma^2) + \frac{ze\beta\zeta}{k_BT} - \frac{2}{3(1+3\overline{\mu}/\mu)}\left[6\gamma(\gamma+\beta) + \frac{4\gamma\Phi^{(1)}(0)}{1-\gamma^2}\right], \tag{2.66}$$

which are the main analytical results of this paper. We further define

$$U_{d,s}^{(0)} = -2\ln(1-\gamma^2) + \frac{ze\beta\zeta}{k_BT}, \tag{2.67a}$$

$$U_{d,l}^{(0)} = -\frac{2}{3(1+3\overline{\mu}/\mu)}\left[6\gamma(\gamma+\beta) + \frac{4\gamma\Phi^{(1)}(0)}{1-\gamma^2}\right] \tag{2.67b}$$

and note that $U_d^{(0)} = U_{d,s}^{(0)} + U_{d,l}^{(0)}$ with $U_{d,s}^{(0)}$ the diffusiophoretic speed of solid particles (Prieve *et al.* 1984). Thus the contribution $U_{d,l}^{(0)}$ is exclusive for drops.

https://doi.org/10.1017/jfm.2018.531 Published online by Cambridge University Press

However, in (2.66), we have not determined $\Phi^{(1)}(0)$, which is the perturbed electric potential of $O(\alpha, \lambda)$ at the interface. Solving for $\Phi^{(1)}$ requires (2.40), (2.48*b*), (2.64*b*) and from appendix A, (A 16), (A 17*b*) and (A 21*b*). Since both $S_b^{(1)}$ and $Q_b^{(1)}$ from appendix A contain an integration with $\mathcal{U}_b^{(1)}$, which is also an integration of $\mathcal{V}_b^{(0)}$, see (A 21*b*), then (2.40) and (2.64*b*) are essentially transcendental equations for $\Phi^{(1)}$ and C_V. Also, a boundary condition for Φ of $O(\alpha, \lambda)$ at the outer edge of the boundary layer is required, which can be partly found in Pawar *et al.* (1993). But note that the result in Pawar *et al.* (1993) is still not precise to $O(\alpha, \lambda)$ because the counterion flux within the boundary layer is neglected and the tangential velocity within the boundary layer $\mathcal{V}_b^0(Y)$ is approximated by the tangential velocity at the outer edge of the boundary layer $\mathcal{V}_b^0(\infty)$. Both simplifications lead to deviations of $O(\alpha, \lambda)$. Therefore, the exact solution for $\Phi^{(1)}(0)$ is not yet determined. It may be easier and more practical to use it as a fitting parameter, which we do when comparing (2.66) with experimental measurements in the next section. The solutions for field variables of different orders and regions are summarized in table 1.

3. Experiments

The diffusiophoresis velocity $U_d^{(0)}$ is the dimensionless velocity of the drop. Since it is scaled by $\boldsymbol{\nabla} \ln c$, $U_d^{(0)}$ can also be deemed as a dimensionless diffusiophoretic mobility (or coefficient), which can further be measured from experiments. To experimentally measure the diffusiophoretic velocity $U_d^{(0)}$ of oil droplets with various viscosities, we perform controlled microfluidics experiments using a dead-end geometry where a solute gradient is established along the dead-end channel and induces approximately rectilinear diffusiophoresis of oil droplets. Detailed experimental methods can be found in our previous papers (Shin *et al.* 2016, 2017*a*). In brief, the charged droplets in a low NaCl concentration solution are introduced to a dead-end pore containing higher NaCl concentration, leading to diffusiophoresis into the dead-end channel. Upon entry, the droplets form a propagating front because the droplet velocity is proportional to the gradient of the logarithmic solute concentration. The colloidal focusing is a function of the diffusiophoretic mobility, which allows us to extract $U_d^{(0)}$ by visualizing the location of the focused region using a fluorescence microscope (DMI4000B, Leica).

The oil emulsions with various viscosities are synthesized by a sonication method (Banerjee *et al.* 2016). In detail, silicone oil (Sigma-Aldrich, 2 cSt $\leqslant \overline{\mu} \leqslant$ 500 cSt) was initially dyed with an oil-soluble fluorescent dye (TP-3400, Tracer Products) at 0.5 vol. %. Then, 1 vol. % of dyed silicone oil was dispersed in an aqueous solution containing 1 mM sodium dodecyl sulfate (SDS) and 1 mM NaCl by vortex stirring (Analog Vortex Mixer, Fisher Scientific) followed by sonication (Ultrasonic Cleaner, Cole-Parmer) for a certain amount of time depending on the viscosity of the oil. The sizes of the oil droplets were measured using a dynamic light scattering device (Zetasizer Nano-ZS, Malvern), where the average diameter was measured as $\approx$0.8 μm. To keep the overall SDS concentration constant during the experiment, so as to neglect migration driven by a surface tension gradient, the same concentration of surfactant (1 mM SDS) was added to the initial solution, which has a high concentration of salt (100 mM NaCl). The zeta potential of the droplets was measured using electrophoretic light scattering (Zetasizer Nano-ZS, Malvern Instruments) and a recently developed diffusiophoretic method (Shin *et al.* 2017*a*), which was measured as ≈ -87 mV regardless of the droplet viscosity.

https://doi.org/10.1017/jfm.2018.531 Published online by Cambridge University Press

https://doi.org/10.1017/jfm.2018.531 Published online by Cambridge University Press

Order	Region	Comment	Field	Formula	Reference
$O(\alpha^0, \lambda^0)$	Outer region	Equilibrium state in the absence of the concentration gradient and drop	Electric potential	$\Psi_{o,0}^{(0)} = \Psi_\infty(0)$	
			Concentration	$C_{o,0}^{(0)} = 1$	
			Velocity	$\mathbf{0}$	
	Boundary layer		Electric potential	$\Psi_{b,0}^{0} = \Psi_\infty(0) + 4\ \mathrm{arctanh}(\gamma \mathrm{e}^{-Y})$	Chew & Sen (1982)
	Drop region	Equilibrium state	Electric potential	$\overline{\Psi}_0^0 = \Psi_\infty(0) + \dfrac{ze\zeta}{k_B T}$	
$O(\alpha^0, \lambda^1)$	Boundary layer	First-order correction by the Debye length	Electric potential	$\Psi_{b,0}^{(1)} = \dfrac{2\gamma \mathrm{e}^{-Y}}{1-\gamma^2 \mathrm{e}^{-2Y}}[\gamma^2(1-\mathrm{e}^{-2Y}) - 2Y]$	Chew & Sen (1982)
$O(\alpha, \lambda^0)$	Outer region	Non-equilibrium state	Electric potential	$\Psi_{o,1}^{(0)}(R,\theta) = -\beta\left(1+\dfrac{1}{2R^3}\right)\boldsymbol{R}\cdot\boldsymbol{e}_x$	
		driven by the concentration gradient	Concentration	$C_{o,1}^{(0)}(R,\theta) = \left(1+\dfrac{1}{2R^3}\right)\boldsymbol{R}\cdot\boldsymbol{e}_x$	
			Velocity	$U_{r,o}^{(0)}(R,\theta) = U_d^{(0)}\left(\dfrac{1}{R^3}-1\right)\cos\theta$	
				$U_{\theta,o}^{(0)}(R,\theta) = U_d^{(0)}\left(\dfrac{1}{2R^3}+1\right)\sin\theta$	
	Boundary layer		Velocity	$U_{r,b}^{(0)} = 0$	Solved by similar methods in Prieve *et al.* (1984)
				$U_{\theta,b}^{(0)}(Y,\theta) = [\,3(1-\beta)[\ln(\mathrm{e}^Y+\gamma) - Y]$	
				$+3(1+\beta)[\ln(\mathrm{e}^Y-\gamma) - Y] + \frac{3}{2}U_d^{(0)}\,]\sin\theta$	
	Drop region	The drop-region flow field is induced by the perturbed charge and electric field on the interface	Velocity	$\overline{U}_r^{(0)} = \overline{a}_4^{(0)}(R^2-1)\cos\theta$	
				$\overline{U}_\theta^{(0)} = -\overline{a}_4^{(0)}(2R^2-1)\sin\theta$	

TABLE 1. The solutions of the concentration, electric and velocity fields of different orders and regions. The expressions for $\overline{a}_4^{(0)}$ and $U_d^{(0)}$ are in (2.65) and (2.66), respectively.

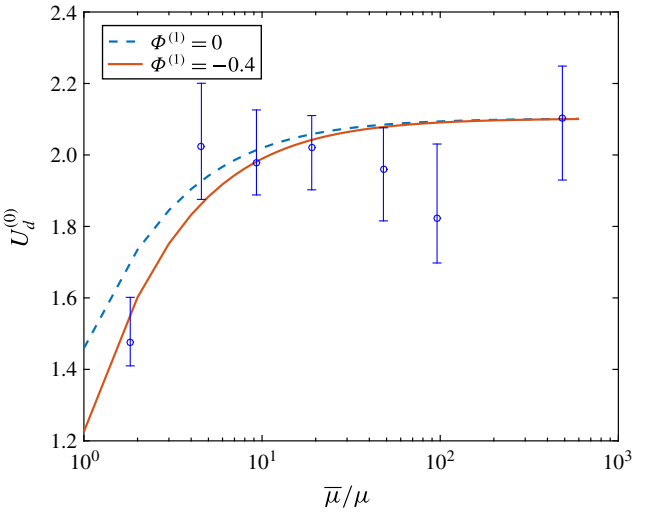

FIGURE 3. (Colour online) The comparison of the analytical results and experiments for the diffusiophoretic velocity as a function of the viscosity ratio $\overline{\mu}/\mu$. The dots and error bars are experimental data. The dotted and solid lines are (2.66), with $\Phi^{(1)} = 0$ and $\Phi^{(1)} = -0.4$, respectively. The electrolyte solution is NaCl with $\beta = -0.208$.

The comparison between the analytical result (2.66) and experimental data is shown in figure 3. If $\Phi^{(1)}(0)$ is neglected in (2.66) (the dotted line in figure 3), we find a small deviation from the experimental data. If $\Phi^{(1)}(0)$ is fitted to be -0.4 (the solid line in figure 3), then the analytical result and experiments are in good agreement. The moderate value for $\Phi^{(1)}(0)$ also shows that treating it as a fitting parameter is practical.

4. Discussion

The diffusiophoretic velocity $U_d^{(0)}$ of silicone oil drops in NaCl solutions is plotted in figure 4. We observe that the diffusiophoretic speed of a droplet converges to its equivalent solid particle as $\overline{\mu}/\mu \to \infty$. In both figures 3 and 4, we notice that there is a small difference between the droplet and solid-particle velocities because the expression of $U_{d,l}^{(0)}$ (2.67*b*) contains a prefactor $(1 + 3\overline{\mu}/\mu)^{-1}$ which decreases as the viscosity ratio $\overline{\mu}/\mu$ increases. The solid-particle result is achieved already by $\overline{\mu}/\mu \simeq 10$.

The velocity fields up to $O(\alpha, \lambda^0)$ in the boundary layer (2.48) are the same for drops and solid particles (Prieve *et al.* 1984) except for an integration constant C_V in (2.48*b*). For solid particles C_V is determined by the no-slip condition on the interface, while for droplets C_V is determined by the stress-balance boundary condition (2.57).

A sketch of the drop-region flow field is shown in figure 5. There is only one parameter $\overline{a}_4^{(0)}$ in the expression of the drop-region flow field (2.56). A change of sign of $\overline{a}_4^{(0)}$ will result in opposite flow directions inside the droplet as shown in figure 5(*a*,*b*). To analyse whether this drop-region flow field will increase or decrease the droplet's diffusiophoretic speed compared with an equivalent solid particle, we first assume the boundary-layer flow is in the positive θ direction (i.e. $U_{d,s}^{(0)} > 0$) for the solid particle, as shown in figure 5(*c*). Then, in the laboratory reference frame,

https://doi.org/10.1017/jfm.2018.531 Published online by Cambridge University Press

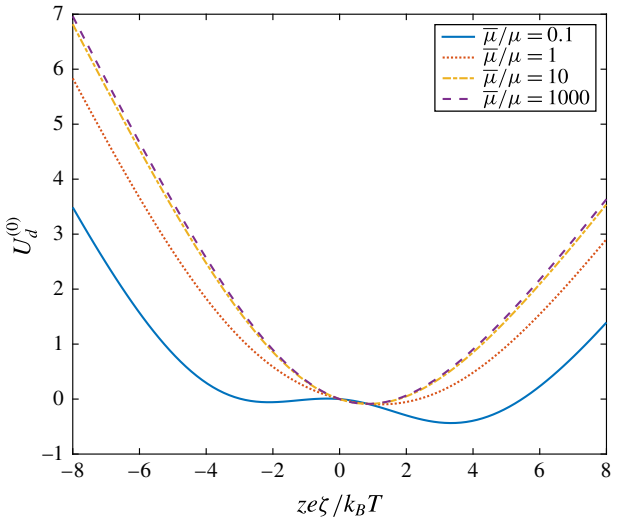

FIGURE 4. (Colour online) The diffusiophoretic velocity in NaCl solutions. The horizontal axis is the dimensionless zeta potential and curves with different viscosity ratios $\overline{\mu}/\mu$ are plotted. $\beta = -0.208$ for NaCl solutions is used and $\Phi^{(1)}$ is neglected.

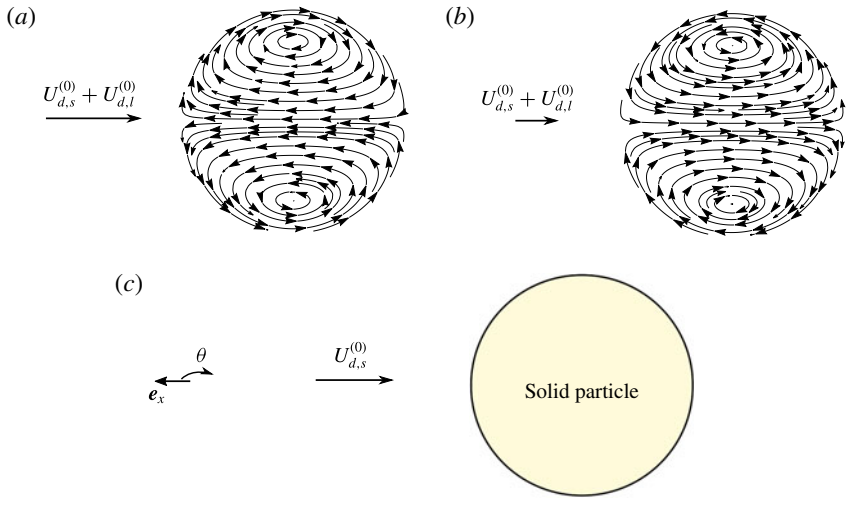

FIGURE 5. (Colour online) The velocity field inside the drop and the migration velocity. All the flow fields are sketched in the drop or solid-particle reference frame. The first two figures are the drop-region velocity field (2.56) with (*a*) $\overline{a}_4^{(0)} = -1$ and (*b*) $\overline{a}_4^{(0)} = 1$ and the uniform flow $U_{d,s}^{(0)} + U_{d,l}^{(0)}$ far away from the drop. (*c*) The far-field flow velocity $U_{d,s}^{(0)}$ outside a solid particle. We fix $U_{d,s}^{(0)} > 0$ for these three cases (i.e. the uniform flow far away from the solid particle (*c*) is in the negative x direction), then the diffusiophoretic speed of drop (*a*) is higher than the solid particle (*c*) because the drop-region flow field is in the same direction as the outer and boundary-layer flow fields. Similarly, the diffusiophoretic speed of drop (*b*) will be lower than that of (*c*).

https://doi.org/10.1017/jfm.2018.531 Published online by Cambridge University Press

this solid particle will move to the left. For a drop, the diffusiophoretic speed will be faster (slower) than its equivalent solid particle if the direction of the drop-region flow field is along the same (opposite) direction of the boundary-layer flow for the solid particle. For example, if $\overline{a}_4^{(0)} = -1$ as in figure 5(*a*), then the drop-region flow is in the same direction as the boundary-layer flow for the solid particle in figure 5(*c*), which will lead to a higher diffusiophoretic speed for droplets to the left in the laboratory reference frame, and *vice versa*.

From (2.62*b*), (2.62*c*), (2.64*a*) and (2.65), we obtain

$$\overline{a}_4^{(0)} = \frac{1}{2(1+3\overline{\mu}/\mu)}(F_0^{(2)}\Phi^{(0)}(0) + F_0^{(1)}\Phi^{(1)}(0)), \tag{4.1}$$

where $F_0^{(1)}$ and $F_0^{(2)}$ are the charge density at $O(\alpha^0, \lambda)$ and $O(\alpha^0, \lambda^2)$ on the interface in (2.61) while $\Phi^{(0)}(0)$ and $\Phi^{(0)}(1)$ are the radial component of the electric potential at $O(\alpha, \lambda^0)$ and $O(\alpha^0, \lambda)$. The appearance of $\Phi(0)$ in (4.1) derives from the tangential electric field in (2.57), i.e.

$$E_{\theta,1} = \frac{1}{R}\frac{\partial \Psi_1}{\partial \theta} = -\Phi(0)\sin\theta \quad \text{at } R = 1, \tag{4.2}$$

where $E_{\theta,1}$ is the tangential electric field at $O(\alpha)$. Also, noticing that the tangential electric field at $O(\alpha^0)$ is zero because Ψ_0 is isotropic, we can conclude that $\overline{a}_4^{(0)}$ is the coefficient of the tangential electric stress FE_θ at $O(\alpha, \lambda^2)$, though with an opposite sign. This result shows that the drop-region velocity field is driven by the tangential electric stress at the interface, and when $F_e E_\theta > 0$, the flow direction at the interface is in the positive θ direction ($\overline{a}_4^{(0)} < 0$) and *vice versa*, which also agrees with the features illustrated in figure 5. By comparing (2.65) with (2.67*b*), we find that

$$U_{d,l}^{(0)} = \tfrac{2}{3}\overline{a}_4^{(0)}, \tag{4.3}$$

i.e. the term exclusive for drops in the expression of $U_d^{(0)}$ is just $\overline{a}_4^{(0)}$ with a constant prefactor. In dimensional terms,

$$\boldsymbol{u}_{d,l}^{(0)} = -\frac{2\epsilon(k_B T)^2}{3(ze)^2(\mu+3\overline{\mu})}\left[6\gamma(\gamma+\beta) + \frac{4\gamma\Phi^{(1)}(0)}{1-\gamma^2}\right]\nabla \ln c, \tag{4.4}$$

which we note is independent of size in this leading-order analysis.

The density of the lightest oil droplets used in our experiment is 0.91 g cm^{-3}. According to Stokes' law, the density difference can generate a sedimentation velocity of $\approx$0.05 μm s^{-1}, which is much smaller than the typical diffusiophoretic speed $\approx$1 μm s^{-1}. In our experiments, gravity is perpendicular to the diffusiophoresis direction. Therefore, the sedimentation should not affect the measurement of diffusiophoretic speeds. In the experiments, the Marangoni effect due to surfactants is singled out by keeping the overall SDS concentration constant. However, the surfactants may 'rigidify' the drop surfaces, e.g. in experiments of settling droplets (Edwards, Brenner & Wasan 1991; Stebe & Maldarelli 1994). As with other phoretic problems, the shear rate at the surface is $O(u/\kappa^{-1})$, which is much larger than the ordinary shear rate $O(u/a)$, associated with translational motion ($(\kappa a)^{-1} \ll 1$). Such large shear rates, and corresponding shear stresses, may be why the interface is not 'rigidified' by surfactant effects (we thank a referee for this idea).

https://doi.org/10.1017/jfm.2018.531 Published online by Cambridge University Press

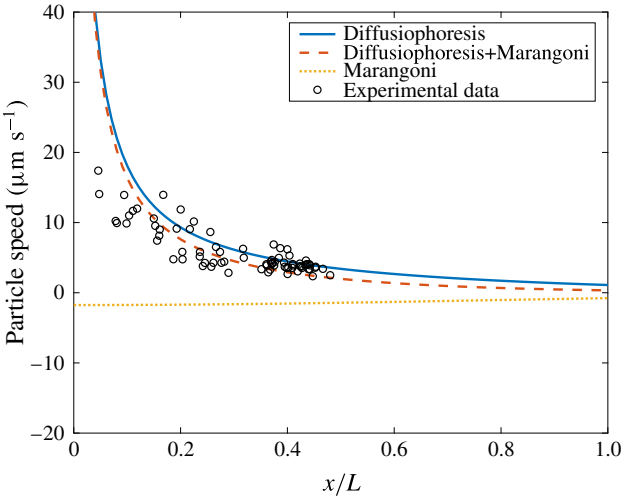

FIGURE 6. (Colour online) Measurement of oil droplet ($\overline{\mu} = 1.82$ mPa s) speeds along the dead-end pore at 10 s after entering, compared with theoretical results of diffusiophoresis and Marangoni effects (calculated using approaches outlined in Shin *et al.* (2016)). x is the entrance distance and $L = 400$ μm is the length of the dead-end pore.

Inside the dead-end pore, the salt gradient can also cause a surface tension gradient and result in a Marangoni velocity. The diffusiophoretic speed is proportional to $\boldsymbol{\nabla} \ln c$, while the Marangoni velocity is proportional to $\boldsymbol{\nabla} c$, and in experiments the Marangoni velocity should be in the opposite direction of diffusiophoresis. As explained in Shin *et al.* (2016), at short times after the oil droplets enter the dead-end pore, the concentration profile along the dead-end pore is approximately an error function. Figure 6 shows the experimental data of velocities for the least viscous oil droplets ($\overline{\mu} = 1.82$ mPa s), whose Marangoni effects should be most significant. Using the approaches in Shin *et al.* (2016), we plot the theoretical results of diffusiophoresis (velocity $\propto \boldsymbol{\nabla} \ln c$) and Marangoni effects (velocity $\propto \boldsymbol{\nabla} c$) and find that the experimental data match with diffusiophoresis theories very well. Therefore, the Marangoni speeds should be at least an order of magnitude slower than the diffusiophoretic speeds. The Marangoni coefficient for silicone oil and water system by adding NaCl is not available in the literature. Based on our analysis, it is predicted to be approximately or less than $O(10^{-4})$ N m^{-1} M.

5. Concluding remarks

In this paper, we use perturbation analysis to solve the concentration, electric and velocity fields for the diffusiophoresis of a charged drop by assuming two small parameters α and λ, the former representing typical concentration changes at the scale of the drop and the latter the dimensionless double layer thickness. The drop-region flow of the drop will induce an additional term $U_{d,l}^{(0)}$ (2.67*b*) in the expression of the diffusiophoretic speed of a drop $U_d^{(0)}$ (2.66) compared with that of a solid particle $U_{d,s}^{(0)}$ (2.67*a*). For the diffusiophoresis of a drop, the continuity of velocity at the interface between the drop and solution requires a drop-region flow field and therefore results in a variation of the surface charge density to balance the viscous stress. Whether the diffusiophoretic speed of a drop is faster or slower than its equivalent solid particle

https://doi.org/10.1017/jfm.2018.531 Published online by Cambridge University Press

depends on the direction of the tangential electric stress at the interface at $O(\alpha, \lambda^2)$. When the stress is in the same direction as the boundary-layer flow outside the equivalent solid particle (e.g. figure 5), the diffusiophoretic speed of the drop will be faster than its equivalent solid particle and *vice versa*.

Acknowledgements

We thank the Princeton Environmental Institute and the National Science Foundation (CBET-1702693) for support. F.Y. is also grateful for support from Princeton University through the George W. Riesz '50 *52 SEAS Fellowship. We thank an anonymous referee for pointing out the surface rigidifying effect.

Appendix A

Here we give details to complete the boundary-layer calculation from § 2.7. In order to solve the velocity fields in the boundary layer, we follow Prieve *et al.* (1984) and define

$$S(R) = \mathcal{C}_+ \mathrm{e}^{\Psi_0 - \Psi_\infty(0)} + \Phi, \tag{A 1a}$$

$$Q(R) = \mathcal{C}_- \mathrm{e}^{-\Psi_0 + \Psi_\infty(0)} - \Phi. \tag{A 1b}$$

Substituting (A 1) into (2.38), we have

$$S'' + \left(\frac{2}{R} - \Psi_0'\right) S' - \frac{2}{R^2} S = (\beta - 1) Pe_b \mathcal{U} \Psi_0', \tag{A 2a}$$

$$Q'' + \left(\frac{2}{R} + \Psi_0'\right) Q' - \frac{2}{R^2} Q = (\beta + 1) Pe_b \mathcal{U} \Psi_0', \tag{A 2b}$$

with four boundary conditions

$$S = (1 - \beta) R \quad \text{as } R \to \infty, \tag{A 3a}$$

$$Q = (1 + \beta) R \quad \text{as } R \to \infty, \tag{A 3b}$$

$$S' = 0 \quad \text{at } R = 1, \tag{A 3c}$$

$$Q' = 0 \quad \text{at } R = 1. \tag{A 3d}$$

We note that equations (A 3*c*) and (A 3*d*) come from the fact that there is no normal ion flux at the interface, i.e. equation (2.9).

The outer solution for S is $S_o = AR^{-2} + (1 - \beta)R$, where A is a constant (note that in the outer region, $\Psi_0' = 0$). We expand $A = A^{(0)} + \lambda A^{(1)} + \lambda^2 A^{(2)} + \cdots$ and substitute $R = 1 + \lambda Y$, so that the outer solution becomes

$$S_o = (A^{(0)} + A^{(1)}\lambda + A^{(2)}\lambda^2 + \cdots)(1 + \lambda Y)^{-2} + (1 - \beta)(1 + \lambda Y) \tag{A 4a}$$

$$= A^{(0)} + 1 - \beta + A^{(1)}\lambda + (1 - \beta - 2A^{(0)})\lambda Y + A^{(2)}\lambda^2 - 2A^{(1)}\lambda^2 Y + \cdots. \tag{A 4b}$$

Also, equation (2.41) can be written as

$$\begin{aligned} \boldsymbol{e}_\phi \cdot \widetilde{\boldsymbol{\nabla}} \wedge \widetilde{\nabla}^2 U_1 &= \frac{\lambda^{-2} \sin\theta \Psi_0'}{2R} (\mathcal{C}_+ - \mathcal{C}_- + 2\cosh[\Psi_0 - \Psi_\infty(0)]\Phi) \\ &= \frac{\lambda^{-2} \sin\theta \Psi_0'}{2R} (S\mathrm{e}^{-\Psi_0 + \Psi_\infty} - Q\mathrm{e}^{\Psi_0 - \Psi_\infty}). \end{aligned} \tag{A 5}$$

https://doi.org/10.1017/jfm.2018.531 Published online by Cambridge University Press

Changing the coordinate variable from R to Y, the functions (A 1) within the boundary layer are defined as

$$S(R) = S(\lambda Y + 1) = S_b(Y), \tag{A 6a}$$
$$Q(R) = Q(\lambda Y + 1) = Q_b(Y). \tag{A 6b}$$

Equations (A 2) in the boundary layer then become

$$\lambda^{-2} S_b'' + \left(\frac{2}{\lambda Y + 1} - \lambda^{-1} \Psi_{b,0}' \right) \lambda^{-1} S_b' - \frac{2}{(\lambda Y + 1)^2} S_b = (\beta - 1) Pe_b \mathcal{U}_b \lambda^{-1} \Psi_{b,0}', \tag{A 7a}$$
$$\lambda^{-2} Q_b'' + \left(\frac{2}{\lambda Y + 1} + \lambda^{-1} \Psi_{b,0}' \right) \lambda^{-1} Q_b' - \frac{2}{(\lambda Y + 1)^2} Q_b = (\beta + 1) Pe_b \mathcal{U}_b \lambda^{-1} \Psi_{b,0}'. \tag{A 7b}$$

Also, equation (A 5) becomes

$$\lambda^{-3} \mathcal{V}_b''' \sin\theta - \frac{2\mathcal{V}_b' \cos\theta}{\lambda(\lambda Y + 1)^2 \sin\theta} + \frac{3\mathcal{V}_b'' \sin\theta}{\lambda^2(\lambda Y + 1)} + \frac{2\mathcal{V}_b \cos\theta}{(\lambda Y + 1)^3 \sin\theta} + \frac{2\mathcal{U}_b \cos\theta}{(\lambda Y + 1)^3} + \frac{\mathcal{U}_b'' \sin\theta}{\lambda^2(\lambda Y + 1)} = \frac{\Psi_{b,0}' \sin\theta}{2\lambda^3(\lambda Y + 1)} (S_b \mathrm{e}^{-\Psi_{b,0} + \Psi_\infty(0)} - Q_b \mathrm{e}^{\Psi_{b,0} - \Psi_\infty(0)}). \tag{A 8}$$

The expansions (in terms of λ) of (A 7a) are

$$(S_b^{(0)})'' - (\Psi_{b,0}^{(0)})'(S_b^{(0)})' = 0, \tag{A 9a}$$

$$(S_b^{(1)})'' + 2(S_b^{(0)})' - (\Psi_{b,0}^{(1)})'(S_b^{(0)})' - (\Psi_{b,0}^{(0)})'(S_b^{(1)})' = (\beta - 1) Pe_b \mathcal{U}_b^{(0)} (\Psi_{b,0}^{(0)})', \tag{A 9b}$$

$$(S_b^{(2)})'' + 2(S_b^{(1)})' - 2Y(S_b^{(0)})' - (\Psi_{b,0}^{(2)})'(S_b^{(0)})' - (\Psi_{b,0}^{(1)})'(S_b^{(1)})' - (\Psi_{b,0}^{(0)})'(S_b^{(2)})'' - 2S_b^{(0)} = (\beta - 1) Pe_b [\mathcal{U}_b^{(0)} (\Psi_{b,0}^{(1)})' + \mathcal{U}_b^{(1)} (\Psi_{b,0}^{(0)})']. \tag{A 9c}$$

Solving (A 9a) with the boundary condition (A 3c) gives

$$(S_b^{(0)})' = 0. \tag{A 10}$$

By matching with the outer solution (A 4b), we have

$$S_b^{(0)} = A^{(0)} + 1 - \beta. \tag{A 11}$$

Using (A 11) and $\mathcal{U}_b^{(0)} = 0$ from (2.48a), we can deduce that $S_b^{(1)}$ is also a constant. By matching $O(\lambda^1)$ and $O(\lambda Y)$ in (A 4b), we have

$$S_b^{(1)} = A^{(1)}, \tag{A 12a}$$
$$1 - \beta - 2A^{(0)} = 0. \tag{A 12b}$$

Together with (A 11), we have

$$S_b^{(0)} = \frac{3(1 - \beta)}{2}. \tag{A 13}$$

Equation (A 9c) then becomes

$$(S_b^{(2)})'' - (\Psi_{b,0}^{(0)})'(S_b^{(2)})' = 2S_b^{(0)} - [2 + (\Psi_{b,0}^{(1)})'](S_b^{(1)})' + (\beta - 1) Pe_b U_1 (\Psi_{b,0}^{(0)})' \tag{A 14}$$

https://doi.org/10.1017/jfm.2018.531 Published online by Cambridge University Press

and the solution is

$$(S_b^{(2)})' = \mathrm{e}^{\Psi_{b,0}^{(0)}-\Psi_\infty(0)} \int_0^Y \mathrm{e}^{-\Psi_{b,0}^{(0)}+\Psi_\infty(0)}[2S_b^{(0)} + (\beta-1)Pe_b\mathcal{U}_b^{(1)}(\Psi_{b,0}^{(0)})']\,\mathrm{d}s + C_s\mathrm{e}^{\Psi_{b,0}^{(0)}-\Psi_\infty(0)}, \tag{A 15}$$

where C_s is an integration constant. The boundary condition (A 3*c*) determines $C_s = 0$. Next, matching with the $O(\lambda^2 Y)$ term in (A 4*b*), we have

$$S_b^{(1)} = A^{(1)} = -\frac{1-\beta}{2}\left[3\int_0^\infty (\mathrm{e}^{-\Psi_{b,0}^{(0)}+\Psi_\infty(0)} - 1)\,\mathrm{d}Y - Pe_b\int_0^\infty \mathcal{U}_b^{(1)}\mathrm{e}^{-\Psi_{b,0}^{(0)}+\Psi_\infty(0)}(\Psi_{b,0}^{(0)})'\,\mathrm{d}Y\right]. \tag{A 16}$$

Similarly, we can solve for the $O(\lambda^0)$ and $O(\lambda^1)$ of Q_b, i.e.

$$Q_b^{(0)} = \frac{3(1+\beta)}{2}, \tag{A 17a}$$

$$Q_b^{(1)} = -\frac{1+\beta}{2}\left[3\int_0^\infty (\mathrm{e}^{\Psi_{b,0}^{(0)}-\Psi_\infty} - 1)\,\mathrm{d}Y + Pe_b\int_0^\infty \mathcal{U}_b^{(1)}\mathrm{e}^{\Psi_{b,0}^{(0)}-\Psi_\infty}(\Psi_0^{(0)})'\,\mathrm{d}Y\right]. \tag{A 17b}$$

The $O(\lambda^0)$ terms in equation (A 8) are

$$(\mathcal{V}_b^{(0)})''' = \frac{(\Psi_{b,0}^{(0)})'}{2}(S_b^{(0)}\mathrm{e}^{-\Psi_{b,0}^{(0)}+\Psi_\infty} - Q_b^{(0)}\mathrm{e}^{\Psi_{b,0}^{(0)}-\Psi_\infty}). \tag{A 18}$$

Integrating (A 18) leads to

$$(\mathcal{V}_b^{(0)})' = -\frac{2S_b^{(0)}\gamma}{\mathrm{e}^Y+\gamma} + \frac{2Q_b^{(0)}\gamma}{\mathrm{e}^Y-\gamma}, \tag{A 19}$$

from which we find

$$\mathcal{V}_b^{(0)} = 2S_b^{(0)}[\ln(\mathrm{e}^Y+\gamma) - Y] + 2Q_b^{(0)}[\ln(\mathrm{e}^Y-\gamma) - Y] + C_V, \tag{A 20}$$

where C_V is a constant. The continuity equation within the boundary layer yields

$$(\mathcal{U}_b^{(0)})' = 0, \tag{A 21a}$$

$$(\mathcal{U}_b^{(1)})' = -2\mathcal{V}_b^{(0)}. \tag{A 21b}$$

Thus $\mathcal{U}_b^{(0)}(Y)$ is constant. In order to satisfy $\mathcal{U}_b(Y=0) = 0$, we have

$$\mathcal{U}_b^{(0)}(Y) = 0. \tag{A 22}$$

https://doi.org/10.1017/jfm.2018.531 Published online by Cambridge University Press

REFERENCES

ANDERSON, J. L. 1989 Colloid transport by interface forces. *Annu. Rev. Fluid Mech.* **21**, 61–99.

ANDERSON, J. L. & PRIEVE, D. C. 1991 Diffusiophoresis caused by gradients of strongly adsorbing solutes. *Langmuir* **7**, 403–406.

BANERJEE, A., WILLIAMS, I., AZEVEDO, R. N., HELGESON, M. E. & SQUIRES, T. M. 2016 Soluto-inertial phenomena: designing long-range, long-lasting, surface-specific interactions in suspensions. *Proc. Natl Acad. Sci. USA* **113** (31), 8612–8617.

BAYGENTS, J. C. & SAVILLE, D. A. 1988 The migration of charged drops and bubbles in electrolyte gradients: diffusiophoresis. *Physico-Chem. Hydrodyn.* **10**, 543–560.

BAYGENTS, J. C. & SAVILLE, D. A. 1991 Electrophoresis of drops and bubbles. *J. Chem. Soc. Faraday Trans.* **87** (12), 1883–1898.

BOOTH, F. 1951 The cataphoresis of spherical fluid droplets in electrolytes. *J. Chem. Phys.* **19**, 1331–1336.

CHEW, W. C. & SEN, P. N. 1982 Potential of a sphere in an ionic solution in thin double layer approximations. *J. Chem. Phys.* **77** (4), 2042–2044.

DERJAGUIN, B. V., SIDORENKOV, G. P., ZUBASHCHENKOV, E. A. & KISELEVA, E. V. 1947 Kinetic phenomena in boundary films of liquids. *Kolloidn. Z.* **9**, 335–347.

DERJAGUIN, B. V., DUKHIN, S. S. & KOROTKOVA, A. A. 1961 Diffusiophoresis in electrolyte solutions and its role in the mechanism of the formation of films from rubber latexes by the method of ionic deposition. *Kolloidn. Z.* **23**, 53–58.

EDWARDS, D. A., BRENNER, H. & WASAN, D. T. 1991 *Interfacial Transport Processes and Rheology*. Butterworth-Heinemann.

FLOREA, D., MUSA, S., HUYGHE, J. M. R. & WYSS, H. M. 2014 Long-range repulsion of colloids driven by ion exchange and diffusiophoresis. *Proc. Natl Acad. Sci. USA* **111** (18), 6554–6559.

HAPPEL, J. & BRENNER, H. 1973 *Low Reynolds Number Hydrodynamics*. Noordhoff International Publishing.

JORDAN, D. O. & TAYLOR, A. J. 1952 The electrophoretic mobilities of hydrocarbon droplets in water and dilute solutions of ethyl alcohol. *Trans. Faraday Soc.* **48**, 346–355.

KAR, A., CHIANG, T., RIVERA, I. O., SEN, A. & VELEGOL, D. 2015 Enhanced transport into and out of dead-end pores. *ACS Nano* **9** (1), 746–753.

KHAIR, A. S. & SQUIRES, T. M. 2009 The influence of hydrodynamic slip on the electrophoretic mobility of a spherical colloidal particle. *Phys. Fluids* **21**, 042001.

LEAL, L. G. 2007 *Advanced Transport Phenomena: Fluid Mechanics and Convective Transport Processes*. Cambridge University Press.

LOU, J. & LEE, E. 2008 Diffusiophoresis of concentrated suspensions of liquid drops. *J. Phys. Chem.* C **112**, 12455–12462.

MANDAL, S., BANDOPADHYAY, A. & CHAKRABORTY, S. 2016 Effect of surface charge convection and shape deformation on the dielectrophoretic motion of a liquid drop. *Phys. Rev.* E **93**, 043127.

OHSHIMA, H. & HEALY, T. W. 1984 Electrokinetic phenomena in a dilute suspension of charged mercury drops. *J. Chem. Soc. Faraday Trans. 2* **80**, 1643–1667.

PAWAR, Y., SOLOMENTSEV, Y. E. & ANDERSON, J. L. 1993 Polarization effects on diffusiophoresis in electrolyte gradients. *J. Colloid Interface Sci.* **155**, 488–498.

PRIEVE, D. C., ANDERSON, J. L., EBEL, J. P. & LOWELL, M. E. 1984 Motion of a particle generated by chemical gradients. Part 2. Electrolytes. *J. Fluid Mech.* **148**, 247–269.

PRIEVE, D. C. & ROMAN, R. 1987 Diffusiophoresis of a rigid sphere through a viscous electrolyte solution. *J. Chem. Soc. Faraday Trans. 2* **83** (8), 1287–1306.

SCHNITZER, O., FRANKEL, I. & YARIV, E. 2014 Electrophoresis of bubbles. *J. Fluid Mech.* **753**, 49–79.

SHIN, S., AULT, J. T., FENG, J., WARREN, P. B. & STONE, H. A. 2017*a* Low-cost zeta potentiometry using solute gradients. *Adv. Mater.* **29**, 1701516.

https://doi.org/10.1017/jfm.2018.531 Published online by Cambridge University Press

SHIN, S., SHARDT, O., WARREN, P. B. & STONE, H. A. 2017*b* Membraneless water filtration using CO_2. *Nat. Commun.* **8**, 15181.

SHIN, S., UM, E., SABASS, B., AULT, J. T., RAHIMI, M., WARREN, P. B. & STONE, H. A. 2016 Size-dependent control of colloid transport via solute gradients in dead-end channels. *Proc. Natl Acad. Sci. USA* **113** (2), 257–261.

STEBE, K. J. & MALDARELLI, C. 1994 Remobilizing surfactant retarded fluid particle interfaces: II. Controlling the surface mobility at interfaces of solutions containing surface active components. *J. Colloid Interface Sci.* **163**, 177–189.

VELEGOL, D., GARG, A., GUHA, R., KAR, A. & KUMAR, M. 2016 Origins of concentration gradients for diffusiophoresis. *Soft Matt.* **12** (21), 4686–4703.

YADAV, V., FREEDMAN, J. D., GRINSTAFF, M. & SEN, A. 2013 Bone-crack detection, targeting, and repair using ion gradients. *Angew. Chem. Intl Ed. Engl.* **52**, 10997–11001.

https://doi.org/10.1017/jfm.2018.531 Published online by Cambridge University Press